V European Conference on Computational Fluid Dynamics
ECCOMAS CFD 2010
J. C. F. Pereira and A. Sequeira (Eds)
Lisbon, Portugal,14-17 June 2010

NUMERICAL SOLUTION OF INCOMPRESSIBLE GENERALIZED NEWTONIAN FLUIDS FLOW

R. Keslerová* and K. Kozel*

*Department of Technical Mathematics, Faculty of Mechanical Engineering,
Czech Technical University in Prague,
Karlovo nám. 13, 121 35 Praha, Czech Republic
e-mail: keslerov@marian.fsik.cvut.cz
e-mail: kozelk@fsik.cvut.cz

Key words: Navier-Stokes equations, Finite volume method, Runge-Kutta method, Artificial compressibility method, dual-time stepping method

Abstract. *This paper deals with the numerical solution of laminar viscous incompressible flows for Newtonian and some non-Newtonian fluids in the branching channel. The mathematical model is the generalized system of Navier-Stokes equations. The finite volume method combined with an artificial compressibility method is used for spatial discretization. For time discretization the explicit multistage Runge-Kutta numerical scheme is considered. Numerical results for steady and unsteady flows for Newtonian and non-Newtonian fluids in two dimensional and three dimensional branching channel are presented.*

1 Introduction

This work deals with the numerical modelling of Newtonian and some non-Newtonian fluids. For the testing the following fluids are used, Newtonian, pseudoplastic (shear thinning) and dilatant (shear thickening). In the Figure 1, the dependence of shear stress and viscosity on the shear rate is shown[7,8].

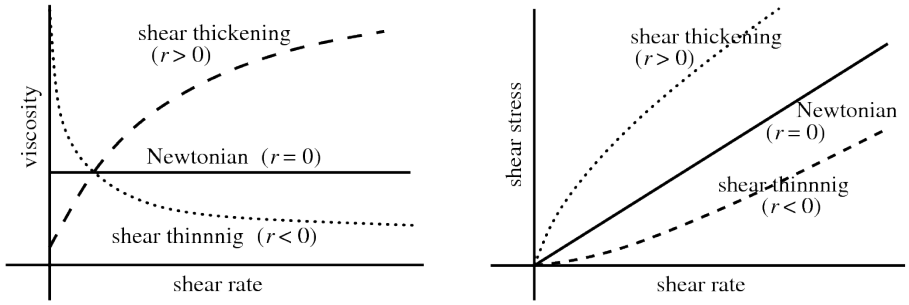

Figure 1: Viscosity and stress of generalized Newtonian fluid as a function of shear rate for power-law fluid

2 Mathematical model

2.1 Generalized Navier-Stokes equations

The fundamental system of equations is the system of Navier-Stokes equations for incompressible fluids. This system of Navier-Stokes equations and the continuity equation for generalized Newtonian fluids can be written in the conservative form[4,1]:

$$\tilde{R}W_t + F^c_x + G^c_y = F^v_x + G^v_y, \quad \tilde{R} = \mathrm{diag}(0,1,1), \tag{1}$$

$$W = \begin{pmatrix} p \\ u \\ v \end{pmatrix}, \quad F^c = \begin{pmatrix} u \\ u^2 + p \\ uv \end{pmatrix}, \quad G^c = \begin{pmatrix} v \\ uv \\ v^2 + p \end{pmatrix}, \tag{2}$$

$$F^v = \begin{pmatrix} 0 \\ \tau_{xx} \\ \tau_{xy} \end{pmatrix}, \quad G^v = \begin{pmatrix} 0 \\ \tau_{yx} \\ \tau_{yy} \end{pmatrix}. \tag{3}$$

where $p = \frac{P}{\rho}$, P is the pressure, u, v are the components of the velocity vector, ρ is the constant density. The vector W is the vector of unknowns. The vectors F^c, G^c are inviscid physical fluxes and F^v, G^v are viscous physical fluxes. The viscous stress τ is defined as follows:

$$\tau = 2\eta(\dot{\gamma})D, \quad \tau = \begin{pmatrix} \tau_{xx} & \tau_{xy} \\ \tau_{yx} & \tau_{yy} \end{pmatrix}, \quad \dot{\gamma} = \sqrt{\mathrm{tr}D^2}, \tag{4}$$

where tensor D is the symmetric part of the velocity gradient and is defined by the relation

$$D = (D)_{ij} = \begin{pmatrix} D_{xx} & D_{xy} \\ D_{yx} & D_{yy} \end{pmatrix}, \quad D_{ij} = \frac{1}{2}\left(\frac{\partial v_i}{\partial x_j} + \frac{\partial v_j}{\partial x_i}\right) \tag{5}$$

where i and j can take on the values x, y or 1, 2. The quantities x_1 and x_2 in the derivatives denote Cartesian coordinates x, y. Similarly v_1 and v_2 denote the velocity vector components u, v.

Newtonian and non-Newtonian fluids differ through the choice of the viscosity function. One of the simplest viscosity function is the power-law model[9].

$$\eta(\dot{\gamma}) = \nu \left(\sqrt{\mathrm{tr} D^2}\right)^r, \tag{6}$$

where ν is a constant, e.g. the kinematic viscosity for Newtonian fluids. The symbol tr D^2 denotes the trace of the tensor D^2. The power r is the power-law index. The power-law model includes Newtonian fluids as a special case ($r = 0$). For $r > 0$ the power-law fluid is shear thickening (increasing viscosity with shear rate), while for $r < 0$ it is shear thinning (decreasing viscosity with shear rate), see Figure 1[3].

3 Numerical solution

3.1 Steady computation

In this first part the steady state solution is considered. In such a case an artificial compressibility method can be applied, i.e. the continuity equation is completed by a term $\frac{1}{\beta^2} p_t$[2,6,10]. In the non-dimensional form this yields

$$\tilde{R}_\beta W_t + F^c_x + G^c_y = \frac{1}{\mathrm{Re}} \epsilon (F^v_x + G^v_y), \quad \tilde{R}_\beta = \mathrm{diag}(\frac{1}{\beta^2}, 1, 1), \quad \beta \in \mathcal{R}^+ \tag{7}$$

where in non-dimensional form

$$W = \begin{pmatrix} p \\ u \\ v \end{pmatrix}, \quad F^c = \begin{pmatrix} u \\ u^2 + p \\ uv \end{pmatrix}, \quad G^c = \begin{pmatrix} v \\ uv \\ v^2 + p \end{pmatrix}, \tag{8}$$

$$F^v = \begin{pmatrix} 0 \\ u_x \\ v_x \end{pmatrix}, \quad G^v = \begin{pmatrix} 0 \\ u_y \\ v_y \end{pmatrix} \tag{9}$$

F^c, G^c are inviscid physical fluxes and F^v, G^v are viscous physical fluxes. The symbol Re denotes Reynolds number and it's defined by the expression

$$\mathrm{Re} = \frac{U^* L^*}{\nu}, \tag{10}$$

where U^*, L^* are the reference velocity and length, ν is the kinematic Newtonian viscosity. The parameter β has dimension of a speed. In the case of non-dimensional equations, β is then divided by a reference velocity U^*. This is usually an upstream velocity, which does not significantly differ from the maximum velocity in the flow field. Hence, in the case of non-dimensional equations, $\beta = 1$ is used in presented steady numerical simulations. The symbol ϵ denotes $\left(\sqrt{\mathrm{tr}D^2}\right)^r$ with used power r equal to 0 (Newtonian fluids) or > 0 (shear thickening fluids) or < 0 (shear thinning fluids).

Eq. (7) is space discretized by the finite volume method[11] and the arising system of ODEs is time discretized by the explicit multistage Runge-Kutta scheme of the second order of accuracy in the time[5]:

$$\begin{aligned} W_i^n &= W_i^{(0)} \\ W_i^{(r)} &= W_i^{(0)} - \alpha_{r-1}\Delta t \mathrm{Res}(W)_i^{(r-1)} \\ W_i^{n+1} &= W_i^{(m)} \qquad\qquad r = 1, \ldots, m, \end{aligned} \tag{11}$$

where $m = 3$, $\alpha_0 = \alpha_1 = 0.5, \alpha_2 = 1.0$, the steady residual $\mathrm{Res}(W)_i$ is defined by finite volume method as

$$\mathrm{Res}(W)_i = \frac{1}{\mu_i} \sum_{k=1}^{4} \left[\left(\overline{F}_k^c - \frac{1}{\mathrm{Re}} \epsilon \, \overline{F}_k^v \right) \Delta y_k - \left(\overline{G}_k^c - \frac{1}{\mathrm{Re}} \epsilon \, \overline{G}_k^v \right) \Delta x_k \right], \tag{12}$$

where μ_i is the volume of the finite volume cell, $\mu_i = \int\int_{C_i} dx \, dy$. The symbols $\overline{F}_k^c, \overline{G}_k^c$ and $\overline{F}_k^v, \overline{G}_k^v$ denote the numerical approximation of the inviscid and viscous physical fluxes. The symbol Re is Reynolds number defined by (10). The symbol ϵ represents $\left(\sqrt{\mathrm{tr}D^2}\right)^r$ The mesh in the considered domain is assumed structured, the finite volume cells are quadrilateral see Figure 2.

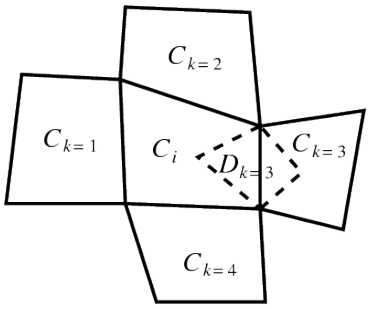

Figure 2: The structure of the finite volume cell and dual volume cell and the neighbouring finite volume cells

The multistage Runge-Kutta scheme (11) is conditionally stable. The time step is chosen to satisfy the CFL coditions

$$\Delta t \leq \min_{i,l} \frac{\mathrm{CFL} \; \mu_i}{\rho_A \Delta y_l + \rho_B \Delta x_l + \frac{2}{\mathrm{Re}} \epsilon \; \left(\frac{(\Delta x_l)^2 + (\Delta y_l)^2}{\mu_i} \right)} \tag{13}$$

index l describes the index of edges coresponds to the finite volume cell C_i. The volume of this cell is μ_i. Δx_l and Δy_l are the lengths of the lth-edge of the cell C_i in the x and y direction. The symbol CFL is so called Courant-Friedrichs-Lewy number for threestage Runge-Kutta method is eual to 2. The Re is Reynolds number defined by 10 and ϵ is $\left(\sqrt{\mathrm{tr}D^2}\right)^r$, where for power r three values are choosed: $r = 0$ for Newtonian fluids, $r = 0.5$ for shear thickening fluids and $r = -0.5$ for shear thinning fluids.

The global behaviour of the solution during the computational process is followed by the L^2 norm of the steady residuum. It is given by

$$\|\mathrm{Res}(W)^n\|_{\mathrm{L}^2} = \sqrt{\sum_i \left(\frac{W_i^{n+1} - W_i^n}{\Delta t}\right)^2} \tag{14}$$

where $\mathrm{Res}(W)^n$ stands for a vector formed by the collection of $\mathrm{Res}(W)_i^n, \forall i$. The decadic logarithm of $\|\mathrm{Res}(W)^n\|_{\mathrm{L}^2}$ is plotted in graphs presenting convergence history of simulation.

3.1.1 Steady boundary conditions

The flow is modelled in a bounded computational domain where the boundary is divided into three mutually disjoint parts: the solid wall, the outlet and the inlet. For two dimensional branching channel the following boundary conditions are considered, see Figure 3

Inlet: At the inlet Dirichlet boundary condition for the velocity vector $(u, v)^T$ is used, pressure inlet value is computed by the extrapolation from the domain's pressure values.

Outlet: At the outlet the pressure value is given and the velocity components u, v are computed by the extrapolation from the domain.

Wall: The homogenous Dirichlet boundary condition for the velocity vector is used on the wall. For the pressure Neumann boundary condition is used.

3.2 Unsteady computation

Two approaches are used for numerical solution of unsteady flows. First, the artificial compressibility method is applied. In this case the artificial compressibility parameter β is set to be a big positive number, ideally $\beta \to \infty$. $\beta = 10$ is used in presented unsteady numerical simulations. In the second aproach dual-time stepping method is used.

The artificial compressibility approach used for unsteady incompressible flows is modifying the system of equations by adding an unsteady term to the continuity equation in the same way as for steady case.

The principle of dual-time stepping method is following. The artificial time τ is introduced and the artificial compressibility method in the artificial time is applied. The

system of Navier-Stokes equations is extended to unsteady flows by adding artificial time derivatives $\partial W/\partial\tau$ to all equations[12,6,10]

$$\tilde{R}_\beta W_\tau + \tilde{R} W_t + F^c_x + G^c_y = F^v_x + G^v_y \tag{15}$$

with matrices $\tilde{R}, \tilde{R}_\beta$ given by Eq. (1), (7). The vector of the variables W, the inviscid fluxes F^c, G^c and the viscous fluxes F^v, G^v are given by Eq. (2).

The derivatives with respect to the real time t are discretized using a three-point backward formula, it defines the form of unsteady residual

$$\tilde{R}_\beta \frac{W^{l+1} - W^l}{\Delta\tau} = -\tilde{R} \frac{3W^{l+1} - 4W^n + W^{n-1}}{2\Delta t} - \mathrm{Res}(W)^l = -\overline{\mathrm{Res}}(W)^{l+1}, \tag{16}$$

where $\Delta t = t^{n+1} - t^n$ and $\mathrm{Res}(W)$ is the steady residual defined as for steady computation, see Eq. (12). The symbol $\overline{\mathrm{Res}}(W)$ denotes unsteady residual. The superscript n denotes the real time index and the index l is associated with the pseudo-time. The integration in pseudo-time can be carried out by explicit multistage Runge-Kutta scheme. The dual-time step $\Delta\tau$ is estimated using Eq. (13). The dual-time step is limited so that $\Delta\tau \leq 2\Delta t/3$.

The solution procedure is based on the assumption that the numerical solution at real time t^n is known. Setting $W^l_i = W^n_i, \forall i$, the iteration in l using explicit Runge-Kutta method are performed until the condition

$$\|\overline{\mathrm{Res}}(W)^l\|_{\mathrm{L}^2} = \sqrt{\sum_i \left(\frac{W^{l+1}_i - W^l_i}{\Delta\tau} \right)^2} \leq \epsilon \tag{17}$$

is satisfied for a chosen small positive number ϵ. The symbol $\overline{\mathrm{Res}}(W)^l$ stands for the vector formed by the collection of $\overline{\mathrm{Res}}(W)^l_i, \forall i$. Once the condition (17) is satisfied for a particular l, one sets $W^{n+1}_i = W^{l+1}_i, \forall i$. Then the index representing real-time level can be shifted one up. History of the convergence of unsteady residual in dual time from t^n to t^{n+1} is plotted in decadic logarithm.

3.2.1 Unsteady boundary condition

The unsteady boundary conditions are defined as follows. In the inlet, in the solid wall and in one of the outlet part the steady boundary conditions are prescribed. In the second outlet part new boundary conditions are defined. The velocity is computed by the extrapolation from the domain. The pressure value is prescribed by the function

$$p_{21} = \frac{1}{4}\left(1 + \frac{1}{2}\sin(\omega t)\right), \tag{18}$$

where ω is the angular velocity defined as $\omega = 2\pi f$, where f is the frequency.

4 Numerical results

In this section the numerical results are presented. The steady numerical results for two dimensional generalized Newtonian fluids are shown in the section 4.1. In the section 4.2 the numerical results for three dimensional branching channel are presented. Last section 4.3 is mentioned to the numerical results of unsteady two dimensional Newtonian fluids.

4.1 Two dimensional steady solution

In this section the steady numerical results of two dimensional incompressible laminar viscous flows for generalized Newtonian fluids are presented. The following choices of the

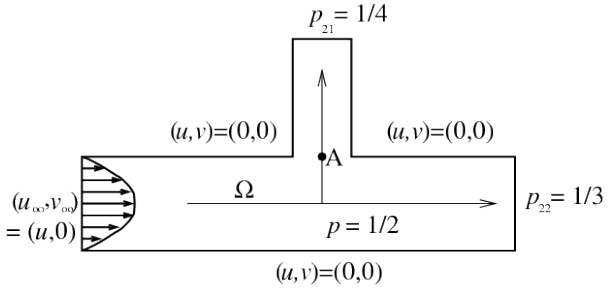

Figure 3: Initial conditions for considered domain

power-law index were used. For Newtonian fluid $r = 0$ is used. For shear thickening and shear thinning non-Newtonian fluid values $r = 0.5$ (shear thickening) and $r = -0.5$ (shear thinning) are used. The flow is computed through the branching channel where the steady boundary condition shown in the Figure 3 are used. In the Figure 3 the initial conditions are sketched. In the inlet the velocity is prescribed by the parabolic function. Reynolds number is equal to 400 for tested cases of the fluids.

In the Figures 4, 5 the velocity isolines and the histories of the convergence for 2D tested fluids are presented. One of the main differencies between Newtonian and non-Newtonian fluids is given by the size of the separation region. From the Figure 4 the separation region is the smallest for shear thickening non-Newtonian fluids and the biggest separation region is for the shear thinning non-Newtonian fluids. Also from the history of the convergence the difference between all considered fluids are clear.

In the Figure 5 the nondimensional axial velocity profile for steady fully developed flow of Newtonian, shear thickening and shear thinning fluids in 2D branching channel is shown.

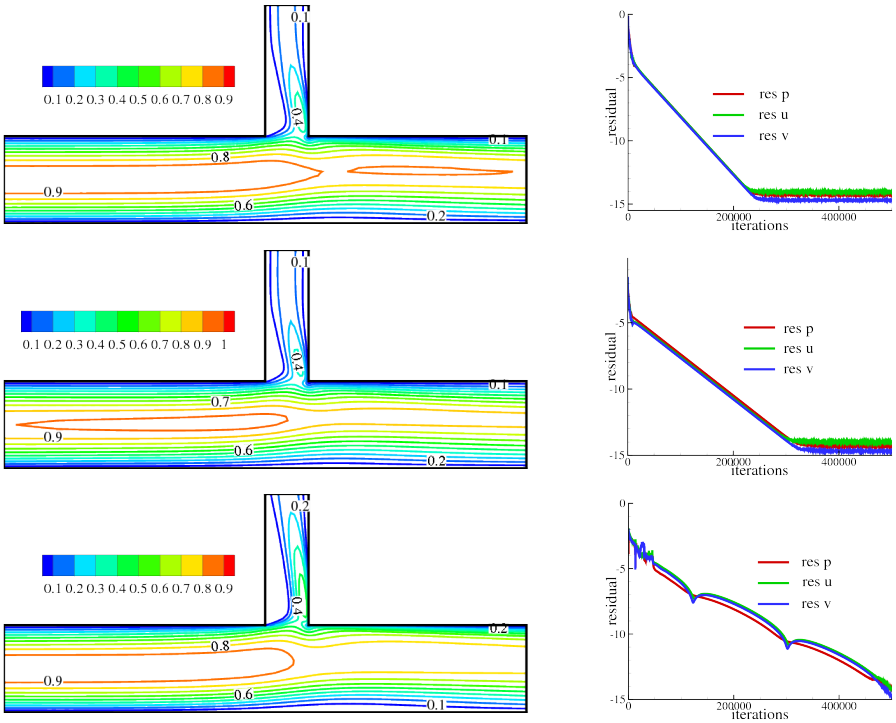

Figure 4: Velocity isolines of steady flows and history of the convergence for generalized Newtonian fluids - a) Newtonian ($r = 0$) - b) shear thickening non-Newtonian ($r = 0.5$) - c) shear thinning non-Newtonian ($r = -0.5$)

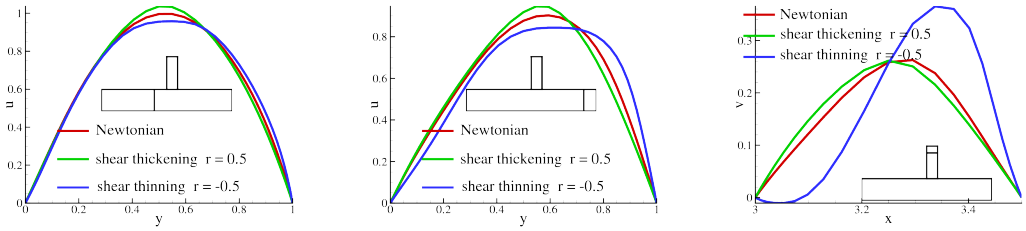

Figure 5: Nondimensional velocity profile for steady fully developed flow of generalized Newtonian fluids in the branching channel

4.2 Three dimensional steady solution

In this section three dimensional steady numerical results for generalized Newtonian fluids are presented. The power-law indices are set as follows: for Newtonian fluid $r = 0$ and for shear thickening $r = 0.5$. The used steady boundary conditions are similar as for two dimensional steady case. The initial data for pressure are the same as for 2D channel. For the velocity vector the constant values at the inlet ($(u, v, w) = (1, 0, 0)$) are used. Reynolds number for tested fluids is 400.

In the Figures 7, 6 velocity isolines for both considered fluids are presented. As for 2D

case the differencies between Newtonian and non-Newtonian are given by the area of the separation region and by the history of the convergence. The separation region is bigger for shear thickening than for Newtonian fluids. In the Figure 8 the cuts through the main channel and through the small branch are shown. The histories of the convergence are presented in the Figure 9. The convergence of the vector of unknowns is slower with increasing power r.

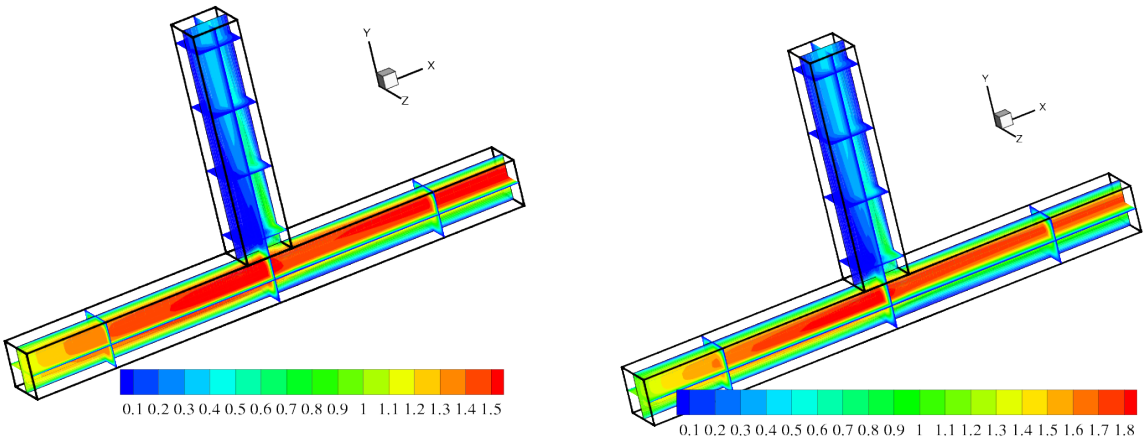

Figure 6: Velocity isolines of steady flows in the branching channel - a) Newtonian ($r = 0$) - b) shear thickening non-Newtonian ($r = 0.5$)

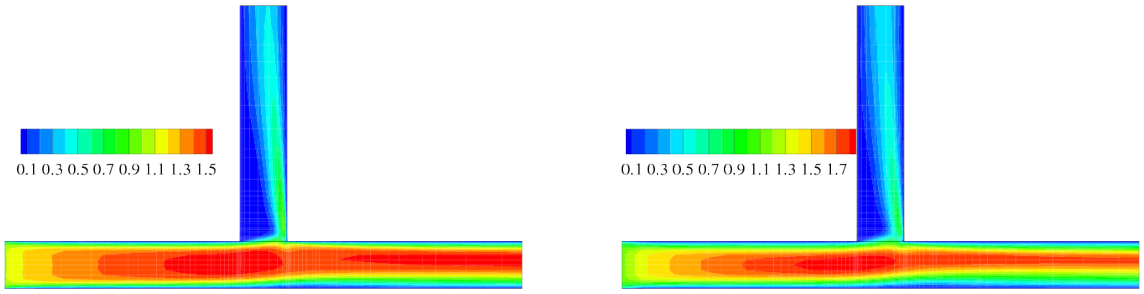

Figure 7: Velocity isolines of steady flows in the branching channel - a) Newtonian ($r = 0$) - b) shear thickening non-Newtonian ($r = 0.5$)

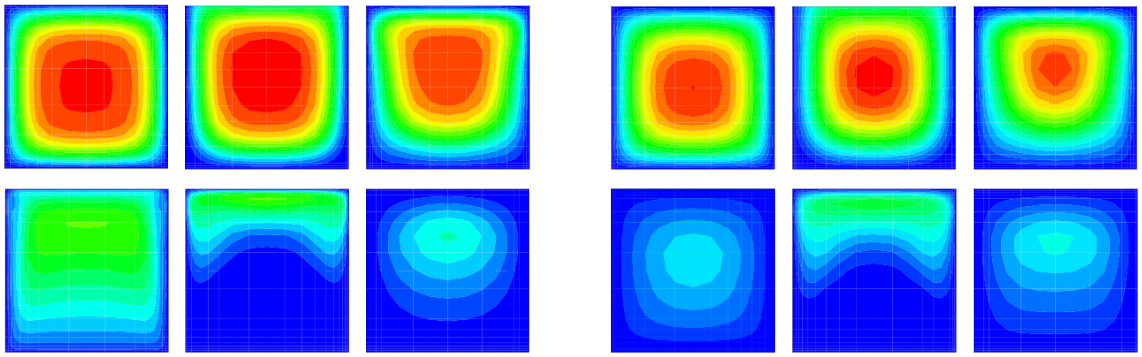

Figure 8: Computed numerical results. Cuts through the main channel (upper) and through the branch (lower) - a) Newtonian ($r = 0$) - b) shear thickening non-Newtonian ($r = 0.5$)

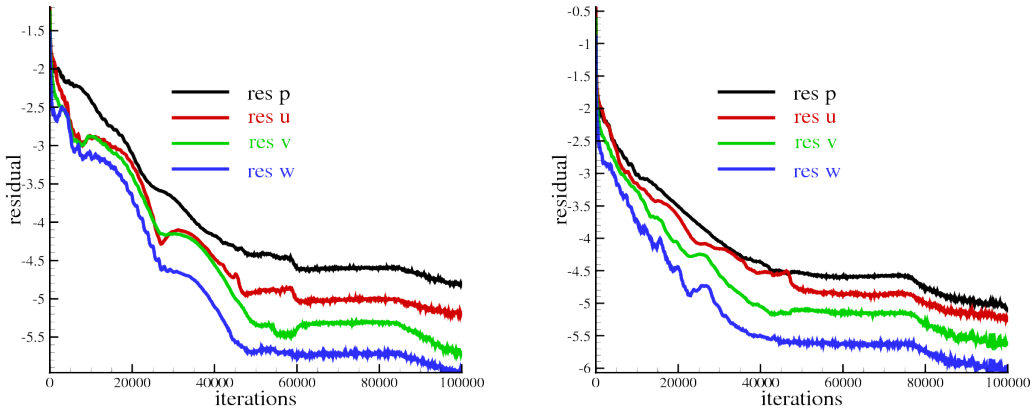

Figure 9: History of the convergence - a) Newtonian - b) shear thickening non-Newtonian ($r = 0.5$)

4.3 Two dimensional unsteady numerical solution

In this section two dimensional unsteady numerical results for Newtonian fluid through the branching channel are presented. The artificial compressibility method and the dual-time stepping method are used. The unsteady boundary conditions defined in the section 3.2 were considered.

4.3.1 Artificial compressibility method

In this subsection the numerical results for Newtonian and considered non-Newtonian fluids are presented. The used unsteady method is the artificial compressibility method. As initial data the numerical solution of steady fully developed flow of generalized Newtonian fluids in the branching channel were used. Reynolds number is 400. The frequency in the pressure function (18) is 2.

In Figures 10 and 11 the graphs of the pressure $p_{21}(t)$ and the velocity in the point

A (see Figure 3) for three tested values of power-law index are shown. By the square symbols the positions of the results shown in the Figures 12, 13 and 14 are sketched.

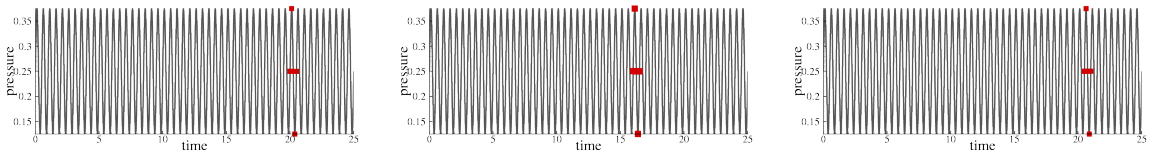

Figure 10: The graphs of the pressure computed by the artificial compressibility method, $\beta = 10$

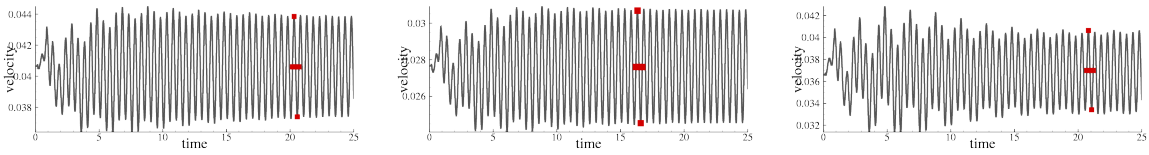

Figure 11: The graphs of the velocity computed by the artificial compressibility method, $\beta = 10$

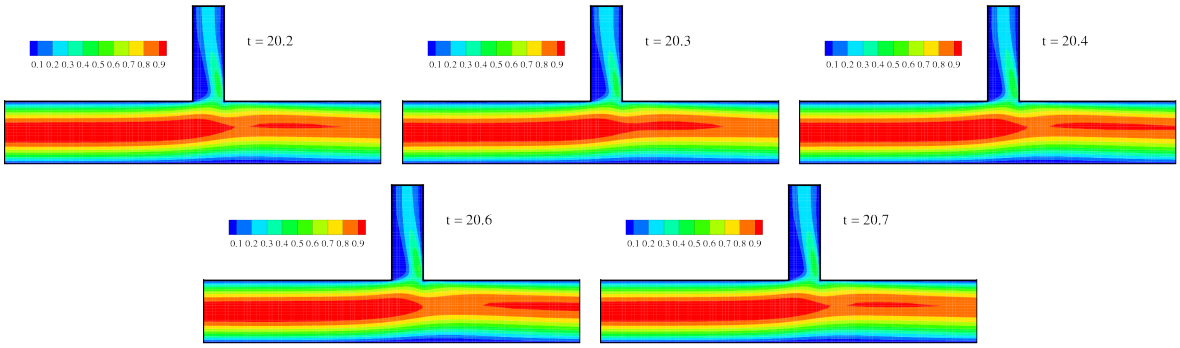

Figure 12: Velocity isolines of unsteady flows of Newtonian fluids

In the Figure 12, 13 and 14 unsteady numerical results during one period for artificial compressibility method and for three tested values of power-law coefficient are presented. Figure 12 shows the unsteady numerical results for Newtonian fluid. In the Figure 13 the unsteady numerical results for shear thickening non-Newtonian fluid with power-law index $r = 0.5$ are presented. Numerical results for shear thinning non-Newtonian fluid are shown in the Figure 14. One can see some differencies during period for all tested fluids as well as differencies between these fluids. From Figure 10 and 11 that the needed time for stabilization is the lowest for shear thickening and with decreasing power-law index the time is increasing.

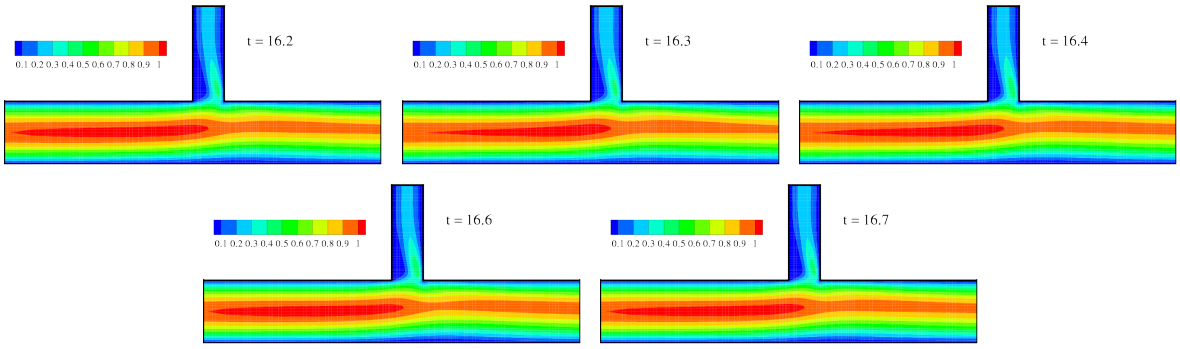

Figure 13: Velocity isolines of unsteady flows of shear thickening non-Newtonian fluids ($r = 0.5$)

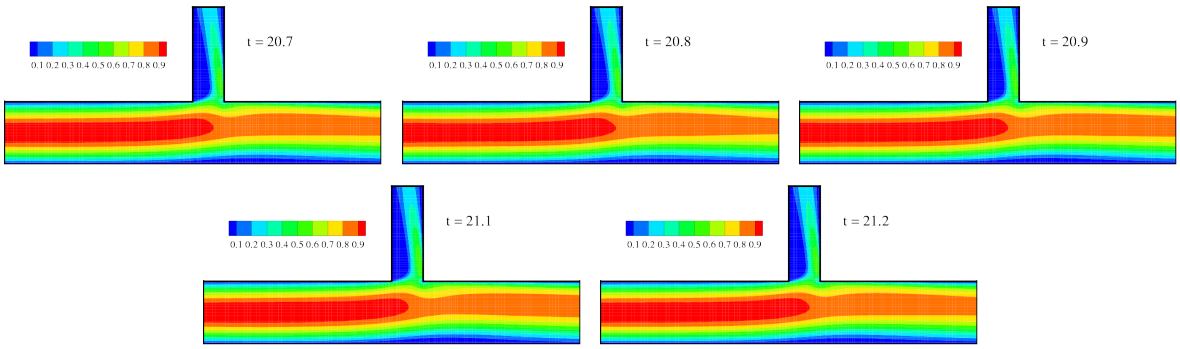

Figure 14: Velocity isolines of unsteady flows of shear thinning non-Newtonian fluids ($r = -0.5$)

4.3.2 Dual-time stepping method

In this subsection the unsteady numerical results for Newtonian are presented. The used unsteady method is the dual-time stepping method. As initial data the numerical solution of steady fully developed flow of Newtonian fluids in the branching channel were used. Reynolds number is 400. The frequency in the pressure function (18) is 2.

In Figure 15 the graphs of the pressure $p_{21}(t)$ and the velocity in the point A (see Figure 3) for Newtonian fluid are shown. By the square symbols the positions of the unsteady numerical results for dual-time stepping method shown in the Figure 16 are sketched.

The decadic logarithm of the L^2 norm of the steady residual in real time is shown in the Figure 16. In the Figure 17 the decadic logarithm of the L^2 norm of unsteady residual by the dual-time stepping method is shown.

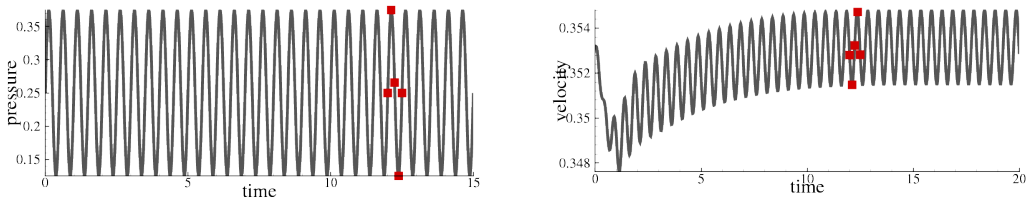

Figure 15: The graphs of the pressure and the velocity computed by the dual-time stepping method

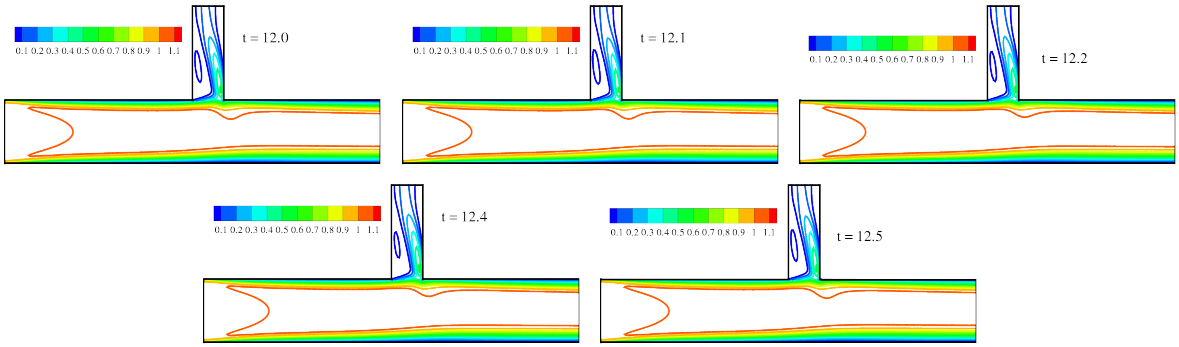

Figure 16: Velocity isolines of unsteady flows of Newtonian fluids - dual-time stepping method

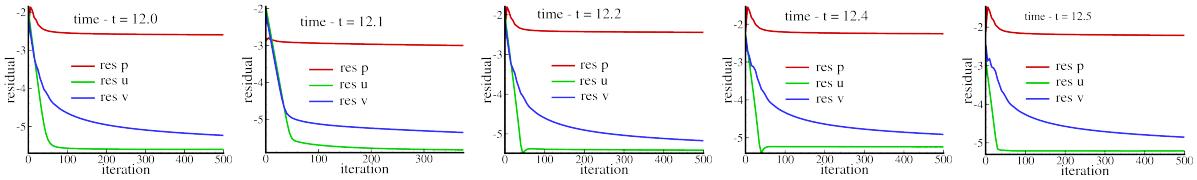

Figure 17: Decadic logarithm of the L^2 norm of the unsteady residual

5 Conclusions

In this paper a finite volume solver for two and three dimensional incompressible laminar viscous flows in the branching channel was described. The numerical results obtained by this method for Newtonian and non-Newtonian (shear thickening and shear thinning) fluid flows were presented. For the generalized Newtonian fluids the power-law model was used. The explicit Runge-Kutta method was considered for numerical modelling. The convergence history confirms the robustness of the applied method.

Acknowledgment

This work was partly supported by grant GAAVCR IAA 100190804 and GACR 101/09/1539, Research Plan MSM 684 077 0003 and Research Plan MSM 684 077 0010.

REFERENCES

[1] R. Dvořák and K. Kozel: *Mathematical Modelling in Aerodynamics (in Czech)*. CTU, Prague, Czech Republic, 1996.

[2] A.J. Chorin, A numerical method for solving incompressible viscous flow problem, *Journal of Computational Physics* **135** 118-125(1967).

[3] T. Bodnar and A. Sequeira, Numerical simulation of the coagulation dynamics of blood, *Computational and Mathematical Methods in Medicine* **4** 83-104(2008).

[4] R. Keslerová and K. Kozel, Numerical Simulations of Incompressible Laminar Flow for Newtonian and Non-Newtonian Fluids (Editor: Springer-Verlag Berlin, Germany), *Numerical Mathematics and Advanced Applications, ENUMATH 2007* 465-472(2008).

[5] A. Jameson and W. Schmidt and E. Turkel, Numerical Solution of the Euler Equations by Finite Volume Methods Using Runge-Kutta Time-Stepping Schemes (Editor: Department of Aeronautics and Astronautics, Stanford USA), *AIAA 14th Fluid and Plasma Dynamic Conference* (1981).

[6] R. Keslerová, *Numerical Solution of Newtonian and Non-Newtonian Flows*. Doctoral dissertation, Czech Technical University, Prague, Czech Republic, 2008.

[7] R.P. Chhabra and J.F. Richardson: *Non-Newtonian Flow in the Process Industries*. Biddles Ltd, Guildford and King's Lynn, Great Britain, 1999.

[8] A.M. Robertson and A. Sequeira and M.V. Kameneva: *Hemorheology*. Birkhäuser Verlag Basel, Switzerland, 2008.

[9] A.M. Robertson: *Review of Relevant Continuum Mechanics*. Birkhäuser Verlag Basel, Switzerland, 2008.

[10] R. Honzátko, *Numerical Simulations of Incompressible Flows with Dynamical and Aeroelastic Effects*. Doctoral dissertation, Czech Technical University, Prague, Czech Republic, 2007.

[11] R. LeVeque: *Finite-Volume Methods for Hyperbolic Problems*. Cambridge University Press, 2004.

[12] A.L. Gaitonde, A Dual-Time Method for two Dimensional Unsteady Incompressible Flow Calculations, *International Journal for Numerical Methods in Engineering* **41** 1153-1166(1998).